J. Fluid Mech. (2010), *vol.* 642, *pp.* 5–14.
doi:10.1017/S0022112009992187

Measurement of cytoplasmic streaming in single plant cells by magnetic resonance velocimetry

JAN-WILLEM VAN DE MEENT[1,2], ANDY J. SEDERMAN[3], LYNN F. GLADDEN[3] AND RAYMOND E. GOLDSTEIN[2]†

[1]Instituut-Lorentz, Universiteit Leiden, Postbus 9506, 2300 RA Leiden, The Netherlands

[2]Department of Applied Mathematics and Theoretical Physics, University of Cambridge, Wilberforce Road, Cambridge CB3 0WA, UK

[3]Department of Chemical Engineering and Biotechnology, University of Cambridge, Pembroke Street, Cambridge CB2 3RA, UK

(Received 6 August 2009; revised 8 September 2009; accepted 10 September 2009; first published online 11 December 2009)

In the giant cylindrical cells found in Characean algae, multitudes of the molecular motor myosin transport the cytoplasm along opposing spiralling bands covering the inside of the cell wall, generating a helical shear flow in the large central vacuole. It has been suggested that such flows enhance mixing within the vacuole (van de Meent, Tuval & Goldstein, *Phys. Rev. Lett.*, vol. 101, 2008, paper no. 178102) and thereby play a role in regulating metabolism. For this to occur the membrane that encloses the vacuole, namely the tonoplast, must transmit efficiently the hydrodynamic shear generated in the cytoplasm. Existing measurements of streaming flows are of insufficient spatial resolution and extent to provide tests of fluid mechanical theories of such flows and information on the shear transmission. Here, using magnetic resonance velocimetry (MRV), we present the first measurements of cytoplasmic streaming velocities in single living cells. The spatial variation of the longitudinal velocity field in cross-sections of internodal cells of *Chara corallina* is obtained with spatial resolution of 16 μm and is shown to be in quantitative agreement with a recent theoretical analysis (Goldstein, Tuval & van de Meent, *Proc. Natl. Acad. Sci. USA*, vol. 105, 2008, p. 3663) of rotational cytoplasmic streaming driven by bidirectional helical forcing in the cytoplasm, with direct shear transmission by the tonoplast. These results highlight the open problem of understanding tonoplast motion induced by streaming. Moreover, this study suggests the suitability of MRV in the characterization of streaming flows in a variety of eukaryotic systems and for microfluidic phenomena in general.

Key words: biological fluid dynamics, low-Reynolds-number flows

1. Introduction

The Characean algae comprise a family of aquatic plants that grow segmented branches, built up from exceptionally large single cells that are several centimetres in length (figure 1). The contents of these cells undergo an active and highly steady circulation known as *cytoplasmic streaming*, driven by the motion of the motor

† Email address for correspondence: R.E.Goldstein@damtp.cam.ac.uk

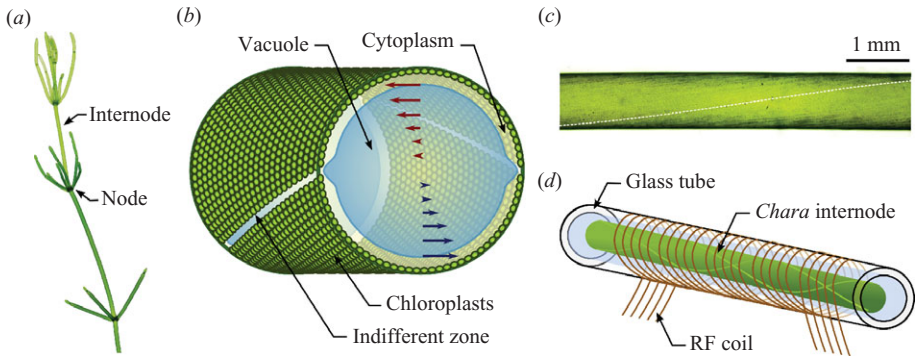

FIGURE 1. Geometry of *Chara corallina*. (*a*) A branch showing internodal cells separated by nodes from which so-called branchlet cells grow in several directions (*b*) Cross-section of a *Chara* internode. Flow is driven in opposing directions along two helical bands separated by indifferent zones visible as light lines on the surface. Velocities are generated in a 10 μm thick layer of cytoplasm at the periphery, but a shear flow extends into the central vacuole that takes up 95 % of the volume of the cell. (*c*) Microscopy image of the sample prior to insertion into the glass tube. The dotted line shows a spiral of dimensionless wavelength $\lambda/R = 42$. (*d*) Schematic of sample holder enclosed in a horizontal radio-frequency (RF) coil. The length of the tube is 40 mm.

protein myosin along bundles of actin filaments at the cell's periphery. Characean cells have been studied since the early days of microscopy (Corti 1774), and the species are recognized as the closest genetic relatives of land plants (Karol *et al.* 2001). Charophytes function as a model system for studies on electrophysiology (Shimmen *et al.* 1994), intercellular transport (Lucas 1995) and carbon fixation in photosynthesis (Lucas 1975).

Cytoplasmic streaming, also known as *cyclosis*, is implicated in transport of nutrients towards regions of growth (Ding *et al.* 1991). It is also hypothesized to aid *homeostasis*, the stable regulation of metabolite concentrations, by enhancing intracellular mixing (Hochachka 1999). In their seminal work on the phenomenon, Kamiya & Kuroda (1956) established that cytoplasmic streaming in Characean algae is driven in the cytoplasm and furthermore that it produces fluid flows that extend throughout the entire vacuole. As pointed out long ago (Pickard 1972) this result implies that the vacuolar membrane (the *tonoplast*) efficiently transmits shear generated in the cytoplasm (Houtman *et al.* 2007) to the vacuole (figure 1*b*). While flow of membranes under shear is well known from the tank-treading of erythrocytes (Fischer, Stohr-Lissen & Schmid-Schonbein 1978), it is clear from recent studies of lipid vesicles under extensional flows (Kantsler, Segre & Steinberg 2007) that sheared membranes can undergo instabilities that lead to complex dynamics. With the ability to image the dynamics of the tonoplast directly in *Arabidopsis* by means of a green-fluorescent-protein-labelled tonoplast integral channel protein (Cutler *et al.* 2000), there is fairly clear evidence that such complex dynamics do take place *in vivo* (Verbelen & Tao 1998), and these may have implications for flows throughout the cell. In *Chara corallina*, for example, the actin–myosin system driving streaming is localized in two opposed helical bands at the cell periphery; the high shear where they meet may create complex tonoplast dynamics.

The possibility that streaming may impact cellular metabolism by mixing the contents efficiently (Hochachka 1999; Pickard 2006) has been revisited recently through solutions of the coupled advection–diffusion dynamics of rotational

cytoplasmic streaming (Goldstein, Tuval & van de Meent 2008; van de Meent, Tuval & Goldstein 2008). These calculations of velocities throughout the vacuole assumed that shear transmission by the tonoplast was complete and showed that vacuolar flows can produce enhanced mixing, providing a possible mechanism for the homeostatic role hypothesized by Hochachka. The first direct measurements of the wall-to-wall velocity profile are those of Kamiya & Kuroda (1956), who studied rhizoid cells, 'leaf' cells sprouting from nodes and internodal cells and found a constant velocity within the cytoplasm and a curved shear profile within the vacuole. Mustacich & Ware (1976) improved on these measurements by using laser-Doppler scattering through a chloroplast-free window obtained by exposure to an argon laser prior to observation. Pickard (1972) obtained velocity measurements for a collection of native particles in an internodal cell of *Chara braunii*, showing consistency with the velocity deduced under the approximation of non-helical indifferent zones.

While existing measurements are compatible with the simplest hydrodynamic descriptions, no full two-dimensional measurements of the cross-sectional flow profiles have been presented to date in any single living cell. Here we report a technical advance in the study of cytoplasmic streaming by obtaining the fluid velocity in internodal cells in *Chara corallina* directly with magnetic resonance velocimetry (MRV). Our results allow for quantitative tests of recent fluid dynamical theories (Goldstein *et al.* 2008; van de Meent *et al.* 2008) and suggest further uses for magnetic resonance imaging (MRI) in the study of large-scale streaming flows.

In recent years, MRI techniques have increasingly found use in non-medical applications (Elkins & Alley 2007), and the advent of phase-shift MRV has made it possible to perform non-invasive flow measurements on microscopic scales (Callaghan 1993). In MRV the initial application of a pulsed magnetic field gradient encodes each spin with a 'label' describing its position along the direction of the gradient. At a time Δ later (the *observation time*), a reversed gradient is applied, introducing a net phase shift in the orientation of the nuclear spin system that is directly related to the distance travelled in the direction of the gradient. By careful selection of the magnitude of the applied field gradients and the observation time, velocities in the range 10^{-5} to $10\,\mathrm{m\,s^{-1}}$ can be measured, depending on fluid properties. The capabilities of MRV have already found application in a range of settings which aid the development and validation of numerical codes or theoretical models, for example the visualization of microfluidics flows (Akpa *et al.* 2007), the imaging of structure and convection in solidifying mushy layers (Aussillous *et al.* 2006), bifurcation phenomena in the flow through a sudden expansion in a circular pipe (Mullin *et al.* 2009) and velocity distributions within a three-dimensional vibro-fluidized bed (Huntley *et al.* 2007). With sufficient time-averaging, spatial resolutions of 10–100 μm can be achieved, allowing imaging of biological systems on scales just slightly larger than those of typical single cells (Choma *et al.* 2006). This has allowed measurements at tissue level in a variety of plant systems (Scheenen *et al.* 2001; Kockenberger *et al.* 2004; Windt *et al.* 2006); it is in the uniquely sized internodes of *Chara* that we can obtain measurements of flows internal to single cells.

2. Cylindrical Stokes flow with helical wall forcing

The Characean internode (figure 1*b*) is a single cylindrical cell with a diameter up to 1 mm and a length that can exceed 10 cm. The bulk of the volume is occupied by a large central vacuole (figure 1*c*) that fulfils a multitude of metabolic roles, acting as storage compartment for sugars, polysaccharides and organic acids, sequestering

toxins such as heavy metals and functioning as a buffering reservoir that helps to maintain ionic and pH homeostasis in the cytoplasm (Taiz 1992). Additionally, the 0.13 M concentration of salts in the vacuolar fluid (Tazawa 1964) produces an outward osmotic pressure of 5 bars that lends the cell its rigidity. At the cell periphery, a layer of cytoplasm roughly 10 μm in thickness encloses the vacuole. In Charophytes most organelles common to higher plants are found in the cytoplasm. Somewhat uniquely, the millions of chloroplasts cover the cell wall, packed into helical rows that spiral along the inner surface (figures 1*b*,*c*). On the inside of those rows, bundled actin filaments act as tracks for myosins that drag structures within the cell (Kachar 1985; Kachar & Reese 1988) and thereby entrain cytoplasm. With streaming rates as high as 100 μm s^{-1}, myosin XI found in *Chara* is the fastest known (Shimmen & Yokota 2004). As a result of a reversed polarity of the actin filaments, the flow is organized in two opposing bands, producing a 'barber-pole' velocity at the cell periphery. These bands are separated by indifferent zones, identifiable by the absence of chloroplasts and visible as two light lines crossing the cell surface.

From a hydrodynamic perspective, the geometry of Characean internodes naturally lends itself to a description as a helical shear flow, where the cytoplasmic bands impose a constant velocity at the boundaries. As typical Reynolds numbers are about 0.03, the problem is most readily treated as a Stokes flow in a cylinder, which can be solved as an expansion in Fourier–Bessel modes (Meleshko, Malyuga & Gomilko 2000). The velocity at the boundary may be used to close the resulting system of linear equations in the coefficients.

For the purposes of studying the flow away from the end points we can approximate the geometry as an infinite cylinder, since the aspect ratio of these cells is generally above 30. This has the advantage that it allows simplification of the problem to a three-dimensional flow with helical symmetry, where the Stokes equations depend only on the radial coordinate r and a helical angle $\varphi = \theta - (2\pi/\lambda)z$, which is the polar angle θ offset by the rotation of the helical bands, with wavelength λ. The problem then reduces to solving the equations

$$\eta \nabla^2 \boldsymbol{u}(r, \varphi) = \nabla p(r, \varphi), \quad \nabla \cdot \boldsymbol{u}(r, \varphi) = 0. \tag{2.1}$$

The basis vectors of the coordinate system can be expressed in terms of the cylindrical coordinates (r, θ, z) as

$$\boldsymbol{e}_r = \boldsymbol{e}_r, \quad \boldsymbol{e}_\varphi = \frac{1}{h}(\boldsymbol{e}_\theta - \kappa r \boldsymbol{e}_z), \quad \boldsymbol{e}_H = \frac{1}{h}(\kappa r \boldsymbol{e}_\theta + \boldsymbol{e}_z), \tag{2.2}$$

where

$$\kappa = \frac{2\pi}{\lambda}, \quad h = \frac{1}{\sqrt{1 + \kappa^2 r^2}}. \tag{2.3}$$

The helical symmetry implies a natural decomposition into a downstream component v along the axis of helical symmetry $\boldsymbol{e}_H$ and the gradient of a streamfunction Ψ containing the transverse components of flow (van de Meent *et al.* 2008):

$$\boldsymbol{u} = v(r, \varphi)\, \boldsymbol{e}_H - \frac{1}{h} \nabla \Psi(r, \varphi) \times \boldsymbol{e}_H. \tag{2.4}$$

The boundary velocity at $r = R$ takes a piecewise constant value U over the top and bottom domains, $\varphi = [0, \pi)$ and $\varphi = [\pi, 2\pi)$. At the indifferent zones located at $\varphi = 0$ and $\varphi = \pi$, the direction of flow reverses over a narrow neighbourhood ϵ of order 10 μm. Rather than approximating the boundary velocity with a step function, with poor convergence of the Fourier expansion because of ringing artefacts, we use

a hyperbolic-tangent dependence near the indifferent zones to obtain a continuous crossover:

$$v(R,\varphi) = \begin{cases} U\tanh(\varphi/\epsilon), & 0 \leqslant \varphi < \pi/2, \\ -U\tanh((\varphi-\pi)/\epsilon), & \pi/2 \leqslant \varphi < 3\pi/2, \\ U\tanh((\varphi-2\pi)/\epsilon), & 3\pi/2 \leqslant \varphi < 2\pi. \end{cases} \tag{2.5}$$

Following Meleshko *et al.* (2000), the hydrodynamic solution can thus be obtained from the boundary conditions as a mode expansion (Goldstein *et al.* 2008). Because of the additional terms in the Laplacian and gradient operators in the helical coordinates, the problem is most easily treated in cylindrical coordinates. The θ and z dependence in the general solution takes the form of a double sum over Fourier modes. In our particular case the symmetry of the problem implies that only combinations of modes that depend on $\varphi = \theta - \kappa z$ contribute to the solution. Performing one of the two sums yields

$$u_r(r,\varphi) = \sum_{n\ \mathrm{odd}} u_r^n(r)\cos(n\varphi), \quad u_\theta(r,\varphi) = \sum_{n\ \mathrm{odd}} u_\theta^n(r)\sin(n\varphi), \tag{2.6a}$$

$$u_z(r,\varphi) = \sum_{n\ \mathrm{odd}} u_z^n(r)\sin(n\varphi), \quad p(r,\varphi) = \sum_{n\ \mathrm{odd}} \eta p^n(r)\cos(n\varphi). \tag{2.6b}$$

The fact that the two bands are identical up to a reversal in the direction of flow implies a pseudo-symmetry $v(R,\varphi) = -v(R,-\varphi)$ in the boundary conditions, which means only the odd terms in the sum need to be considered.

To find the radial modes, we write $u_r^n = -(a^n + b^n)/2$ and $u_\theta^n = -(a^n - b^n)$, after which the solution takes the form of a combination of modified Bessel functions,

$$a_r^n(r) = \frac{1}{I_n(n\kappa R)}\left[A^n I_{n+1}(n\kappa r) + P^n\frac{\kappa r}{2\pi}I'_{n+1}(n\kappa r)\right], \tag{2.7a}$$

$$b_r^n(r) = \frac{1}{I_n(n\kappa R)}\left[B^n I_{n-1}(n\kappa r) + P^n\frac{\kappa r}{2\pi}I'_{n-1}(n\kappa r)\right], \tag{2.7b}$$

$$u_z^n(r) = -\frac{1}{I_n(n\kappa R)}\left[C^n I_n(n\kappa r) + P^n\frac{\kappa r}{2\pi}I'_n(n\kappa r)\right], \tag{2.7c}$$

$$p_r^n(r) = -\frac{1}{I_n(n\kappa R)}\left[P^n\frac{\kappa}{\pi}I_n(n\kappa r)\right]. \tag{2.7d}$$

The form above satisfies the momentum equation. The coefficients A^n, B^n and C^n can now be obtained from the boundary conditions, by using the continuity equation to relate the coefficients for the pressure to the components of flow: $P^n = -n\pi(A^n + B^n - 2C^n)$. One may verify that in the limit $\lambda \to \infty$, where the indifferent zones are straight, a cylindrically symmetric solution is obtained,

$$u_z(r,\theta) = \sum_{n\ \mathrm{odd}} D^n r^n \sin n\theta. \tag{2.8}$$

A step-function boundary velocity yields the solution that is due to Pickard (1972),

$$u_z(r,\theta) = \frac{2U}{\pi}\arctan\frac{2(r/R)\sin\theta}{1-(r/R)^2}. \tag{2.9}$$

In the general case, the resulting linear system of equations can be readily solved using linear algebra software, after which the forms $v(r,\phi)$ and $\Psi(r,\phi)$ are obtained by a transformation from the solution in cylindrical coordinates. The streamfunction

components, which potentially play a role in the enhancement of intracellular mixing in younger cells, are expected to have a magnitude of less than 1 μm s^{-1} in mature internodal cells whose helical wavelength is typically quite long (10–30 mm). Such speeds are below the effective noise limit of the MRV measurements. Our experiments do however provide a comparison with the downstream profile to an extent not previously possible, allowing us to examine the degree to which the vacuolar flow is consistent with constant imposed velocity at the boundary.

In the results presented here, 64 modes were used for the expansion. The crossover width was equivalent to $\epsilon = 11$ μm. To allow comparison with the MRV measurements, which obtain the mean flow along a volume of several millimetres along the z-axis, a series of profiles was averaged along a length of 3 mm, using a Gaussian weighting with a spread of 1 mm full-width at half-maximum (FWHM), as was used in the experiments.

3. Magnetic resonance velocimetry measurements

Our experiments were performed on internodes excised from *Chara corallina* var. *australis*, originally obtained from the Botanic Garden of the University of Cambridge, courtesy of J. Banfield. The plants were grown in a non-axenic culture, rooted in non-fertilized soil in a 100 l tank filled with artificial pond water (1 mM NaCl, 0.4 mM KCl, 0.1 mM $CaCl_2$). The tank was kept at room temperature and illuminated with a 2700 K fluorescent lamp on a 16/8 h day–night cycle. During illumination, the light intensity at the top of the tank was 7 μmol $m^{-2}s^{-1}$. Samples of suitable size were placed in a Petri dish under a microscope to verify healthy streaming.

To measure the cross-sectional flow inside the internodal vacuole, a sample was inserted into a horizontal solenoidal radio-frequency (RF) coil (figure 1*d*), in a glass capillary of diameter 1.6 mm and length 40 mm, which was pre-filled with Forsberg medium (Forsberg 1965). The capillary tube was closed with polydimethylsiloxane (PDMS) plugs and a small volume of silicone grease to ensure a good seal over the measurement time of 192–256 min needed to obtain the cross-sectional resolutions of 16 μm × 31 μm in our experiments.

Velocimetry measurements were performed on a Bruker Spectrospin DMX 200, 4.7 T magnet with a 20 mm long solenoid coil of diameter 3 mm; ^{1}H images were acquired at 199.7 MHz. Spatial resolution was achieved using three-axis shielded gradient coils providing a maximum gradient strength of 49 G cm^{-1} in each direction. Transport is measured over the observation time, Δ, and since the root mean square displacement increases as $\Delta^{1/2}$ because of diffusion and as Δ^1 because of convection, for short Δ diffusive (incoherent) displacements can dominate over convective (coherent) ones, particularly in slowly convecting systems. Therefore, to weight the measurement towards the convective field a stimulated echo sequence was used to enable a large observation time for motion encoding. Further spatial imaging gradients were applied after the motion encoding to minimize diffusive attenuation. Hard 90° RF pulses were used except for the final pulse which was a Gaussian-shaped selective 90° RF pulse 512 μs in duration. Experimental parameters used for the velocity images were as follows: observation time, $\Delta = 500$ ms; velocity gradient duration, $\delta = 1.62$ ms; gradient increment, $g_{inc} = 10$ G cm^{-1}; number of velocity gradient increments = 2; recycle time, $TR = 1.9$ s; number of scans = 16; field of view = 2 mm × 2 mm; pixel array size $N_{read} \times N_{phase} = 128 \times 64$; in-plane spatial resolution = 16 μm × 31 μm; slice thickness = 1 mm; measurement duration = 64 min.

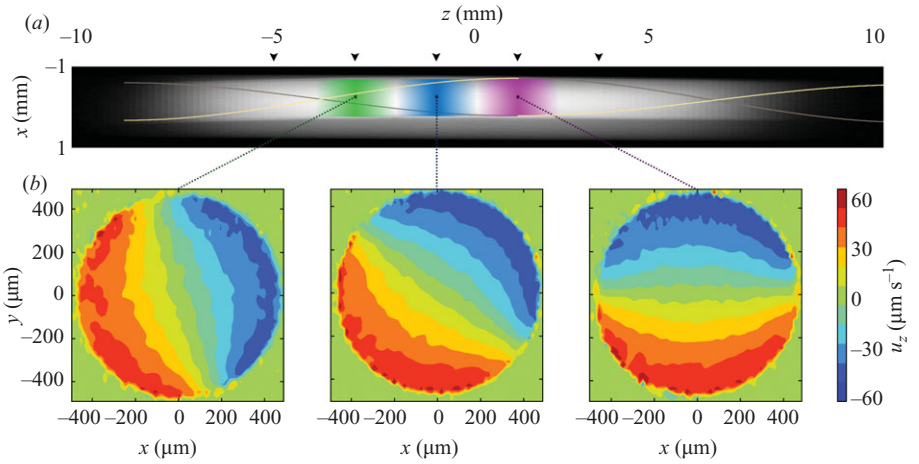

FIGURE 2. MRV measurements of the cross-sectional velocity profile of *Chara corallina*. (*a*) Nuclear magnetic resonance (NMR) image of the sample, with the measurement volumes at $z = -3$ mm, -1 mm, 1 mm, respectively marked in green, blue and magenta. The dotted lines mark the extrapolated position of the indifferent zones, as determined from the orientation of the velocity profiles at five measurement points between $z = -5$ mm and $z = 3$ mm (marked with black arrowheads). (*b*) Cross-sectional plots of the velocity. The resolutions along the *x*- and *y*-axis are 16 μm and 31 μm respectively. Measurements were averaged along the *z*-axis over a Gaussian-weighted region of width 1 mm (FWHM). The fitted maximum velocities are 45.2 μm s^{-1}, 46.0 μm s^{-1} and 46.9 μm s^{-1}.

For each data set, four measurements were taken 3–7 h apart and were subsequently averaged. A Gaussian smoothing with 31 μm FWHM was selectively applied to the streaming region while avoiding blurring at the cell periphery. The streaming velocity in the individual measurements was not observed to vary significantly over the 15 h period of acquisition. Throughout the measurements the temperature was maintained at 298 K by a regulated airflow system.

Figure 2(*a*) shows the location of the five averaging domains on a particular sample, and figure 2(*b*) shows the velocity profiles at three of those positions. Mean flow velocities are ∼45 μm s^{-1}, which is roughly consistent with other measurements for a cell of radius $R = 460$ μm at the temperature of 298 K (Pickard 1974), though the low ambient light levels inside the coil may have reduced the streaming rate somewhat (Plieth & Hansen 1992). The helical pitch obtained from five short measurements 2 mm apart (figure 2*a*, arrowheads) is 18.6° mm^{-1}, giving a dimensionless wavelength of $\lambda/R = 42.0$, in good agreement with our estimate from the light-microscopy image in figure 1(*b*).

Aligning and averaging the three data sets in figure 2(*b*) we further enhance the signal-to-noise ratio of the profile. The resulting cross-section (figure 3*a*) is in excellent agreement with the hydrodynamic solution, shown in figure 3(*b*). As indicated in the previous section, we account for the ∼20° of helical rotation along the measurement volume by averaging the theoretical expression over a length of 3 mm with the same Gaussian weighting as the MRV measurements. The wall-to-wall one-dimensional profiles in figure 3(*c*) show close agreement with the theoretical solution. In figure 3(*d*), measurement points are plotted against their theoretical values, in the manner of earlier velocity measurements (Pickard 1972). The colour of the points indicates the radial distance from the centre of the cell. We see a remarkably good correspondence

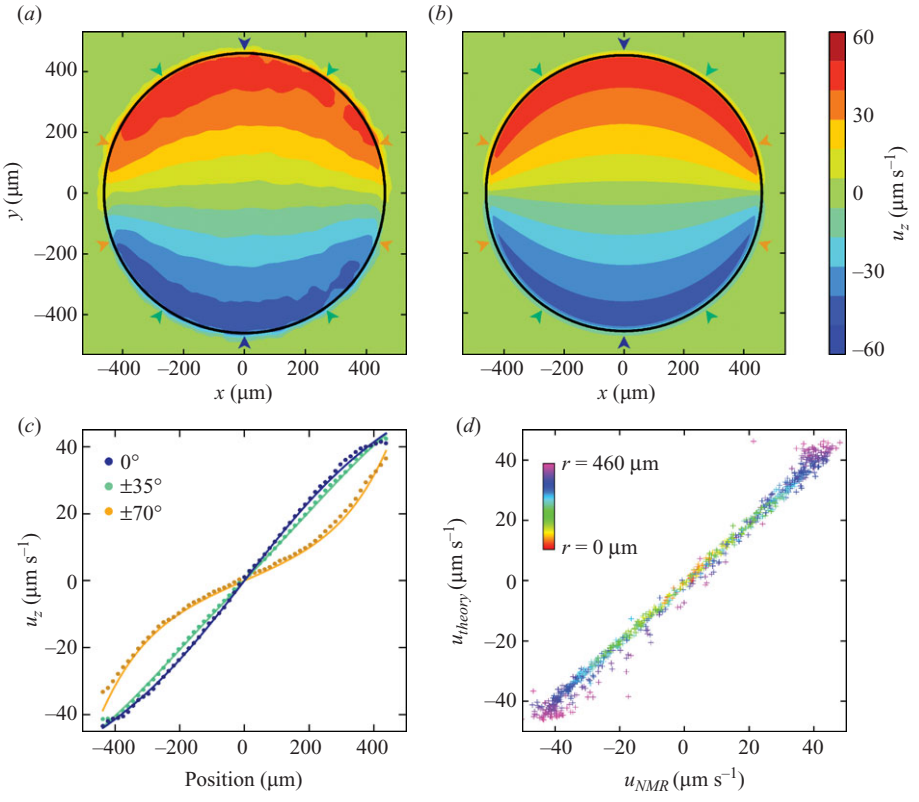

FIGURE 3. Comparison between measurements and theoretical solution. (*a*) Reconstructed profile created by aligning and averaging the data sets shown in figure 2(*b*). The black circle shows the position of the cell wall. (*b*) Corresponding theoretical profile. (*c*) Three wall-to-wall velocity sections at orientations of 0°, ±35° and ±70° with respect to the *y*-axis (see arrowheads in panels above). For non-zero angles the data is averaged over the section with positive and negative orientation. The markers show the measured values, and the lines show the theoretical prediction. (*d*) Comparison between measurements and theoretical values. Data points from all three profiles are shown as markers, with the colour of the marker denoting the radial position of the data. For clarity, only 1 in 10 points is shown.

throughout the bulk of the cell, with deviations restricted primarily to points within a pixel from the cell wall, where partial-volume effects become significant.

In summary, we have established that the cytoplasmic streaming velocity field within a particular plant cell is consistent with direct transmission of shear through the vacuolar membrane. It is therefore accurate to represent the driving force from the actin–myosin system within the cytoplasm as a piecewise constant Dirichlet condition of specified velocity at the cell periphery. The clear implication of this result is that the tonoplast itself is carried along with the flow in each of the two hemicylinders of the cell. As the streaming velocities can reach 100 μm s^{-1} in the two directions, and the transition region at the indifferent zones is ∼20 μm wide, the shear rate experienced by the membrane there can reach the rather large value of 10 s^{-1}. Further work is needed to understand the membrane dynamics there and to determine the manner in which the complex rheology of the cytoplasm is coupled with the tonoplast. On a more general level, these measurements show that MRV can yield detailed information on the velocity distribution of cytoplasmic streaming within single plant cells, allowing

quantitative comparison with fluid dynamical theories. Natural extensions of this work include studies of other streaming geometries found to elucidate the nature of their forcing by molecular motors and the study of tracer particle dynamics as a probe of mixing (Esseling-Ozdoba *et al.* 2008).

The authors thank M. Polin, T. J. Pedley, C. Picard and I. Tuval for numerous discussions. J. W. van de Meent gratefully acknowledges the support of the EPSRC and Leiden University. The work of A. J. Sederman and L. F. Gladden was supported in part by the EPSRC grant EP/F047991/1, and R. E. Goldstein acknowledges partial support from the Leverhulme Trust and the Schlumberger Chair Fund.

REFERENCES

Akpa, B. S., Matthews, S. M., Sederman, A. J., Yunus, K., Fisher, A. C., Johns, M. L. & Gladden, L. F. 2007 Study of miscible and immiscible flows in a microchannel using magnetic resonance imaging. *Anal. Chem.* **79**, 6128–6134.

Aussillous, P., Sederman, A. J., Gladden, L. F., Huppert, H. E. & Worster, M. G. 2006 Magnetic resonance imaging of structure and convection in solidifying mushy layers. *J. Fluid Mech.* **552**, 99–125.

Callaghan, P. T. 1993 *Principles of Nuclear Magnetic Resonance Microscopy*. Clarendon.

Choma, M. A., Ellerbee, A. K., Yazdanfar, S. & Izatt, J. A. 2006 Doppler flow imaging of cytoplasmic streaming using spectral domain phase microscopy. *J. Biomed. Opt.* **11**, 024014.

Corti, B. 1774 *Osservazione Microscopische sulla Tremella e sulla Circulazione del Fluido in Una Planto Acquaguola*. Appresso Giuseppe Rocchi.

Cutler, S. R., Ehrhardt, D. W., Griffitts, J. S. & Somerville, C. R. 2000 Random GFP::cDNA fusions enable visualization of subcellular structures in cells of Arabidopsis at a high frequency. *Proc. Natl. Acad. Sci. USA* **97**, 3718–3723.

Ding, D. Q., Mimura, T., Amino, S. & Tazawa, M. 1991 Intercellular transport and photosynthetic differentiation in *Chara corallina*. *J. Exp. Bot.* **42**, 33–38.

Elkins, C. J. & Alley, M. T. 2007 Magnetic resonance velocimetry: applications of magnetic resonance imaging in the measurement of fluid motion. *Exp. Fluids* **43**, 823–858.

Esseling-Ozdoba, A., Houtman, D., van Lammeren, A. A. M., Eiser, E. & Emons, A. M. C. 2008 Hydrodynamic flow in the cytoplasm of plant cells. *J. Microscopy* **231**, 274–283.

Fischer, T. M., Stohr-Lissen, M. & Schmid-Schonbein, H. 1978 The red cell as a fluid droplet: tank tread-like motion of the human erythrocyte membrane in shear flow. *Science* **202**, 894–896.

Forsberg, C. 1965 Nutritional studies of *Chara* in axenic cultures. *Physiol. Plantarum* **18**, 275–290.

Goldstein, R. E., Tuval, I. & van de Meent, J. W. 2008 Microfluidics of cytoplasmic streaming and its implications for intracellular transport. *Proc. Natl. Acad. Sci. USA* **105**, 3663–3667.

Hochachka, P. W. 1999 The metabolic implications of intracellular circulation. *Proc. Natl. Acad. Sci. USA* **96**, 12233–12239.

Houtman, D., Pagonabarraga, I., Lowe, C. P., Esseling-Ozdoba, A., Emons, A. M. C. & Eiser, E. 2007 Hydrodynamic flow caused by active transport along cytoskeletal elements. *Europhys. Lett.* **78**, 18001.

Huntley, J. M., Martin, T. W., Mantle, M. D., Shattuck, M. D., Sederman, A. J., Wildman, R. D., Gladden, L. F. & Halliwell, N. A. 2007 NMR measurements and hydrodynamics simulations of phase-resolved velocity distributions within three-dimensional vibrofluidized granular bed. *Proc. R. Soc.* A **463**, 2519–2542.

Kachar, B. 1985 Direct visualization of organelle movement along actin filaments dissociated from characean algae. *Science* **227** (4692), 1355–1357.

Kachar, B. & Reese, T. S. 1988 The mechanism of cytoplasmic streaming in characean algal cells: sliding of endoplasmic reticulum along actin filaments. *J. Cell Biol.* **106**, 1545–1552.

Kamiya, N. & Kuroda, K. 1956 Velocity distribution of the protoplasmic streaming in *Nitella* cells. *Bot. Mag. Tokyo* **69**, 544–554.

Kantsler, V., Segre, E. & Steinberg, V. 2007 Vesicle dynamics in time-dependent elongation flow: wrinkling instability. *Phys. Rev. Lett.* **99**, 178102.

Karol, K. G., McCourt, R. M., Cimino, M. T. & Delwiche, C. F. 2001 The closest living relatives of land plants. *Science* **294**, 2351–2353.

Kockenberger, W., De Panfilis, C., Santoro, D., Dahiya, P. & Rawsthorne, S. 2004 High resolution NMR microscopy of plants and fungi. *J. Microscopy* **214**, 182–189.

Lucas, W. J. 1975 Photosynthetic fixation of ^{14}carbon by internodal cells of *Chara corallina*. *J. Exp. Bot.* **26**, 331–346.

Lucas, W. J. 1995 Plasmodesmata: intercellular channels for macromolecular transport in plants. *Curr. Op. Cell Biol.* **7**, 673–680.

van de Meent, J. W., Tuval, I. & Goldstein, R. E. 2008 Nature's microfluidic transporter: rotational cytoplasmic streaming at high Péclet numbers. *Phys. Rev. Lett.* **101**, 178102.

Meleshko, V. V., Malyuga, V. S. & Gomilko, A. M. 2000 Steady stokes flow in a finite cylinder. *Proc. R. Soc.* A **456**, 1741–1758.

Mullin, T., Seddon, J. R. T., Mantle, M. D. & Sederman, A. J. 2009 Bifurcation phenomena in the flow through a sudden expansion in a circular pipe. *Phys. Fluids* **21**, 014110.

Mustacich, R. V. & Ware, B. R. 1976 A study of protoplasmic streaming in *Nitella* by laser Doppler spectroscopy. *Biophys. J.* **16**, 373–388.

Pickard, W. F. 1972 Further observations on cytoplasmic streaming in *Chara braunii*. *Can. J. Bot.* **50**, 703–711.

Pickard, W. F. 1974 Hydrodynamic aspects of protoplasmic streaming in *Chara braunii*. *Protoplasma* **82**, 321–339.

Pickard, W. F. 2006 Absorption by a moving spherical organelle in a heterogeneous cytoplasm: implications for the role of trafficking in a symplast. *J. Theoret. Biol.* **240**, 288–301.

Plieth, C. & Hansen, U. P. 1992 Light dependence of protoplasmic streaming in *Nitella flexilis* L. as measured by means of laser-velocimetry. *Planta* **188**, 332–339.

Scheenen, T. W. J., Vergeldt, F. J., Windt, C. W., de Jager, P. A. & Van As, H. 2001 Microscopic imaging of slow flow and diffusion: a pulsed field gradient stimulated echo sequence combined with turbo spin echo imaging. *J. Mag. Res.* **151**, 94–100.

Shimmen, T., Mimura, T., Kikuyama, M. & Tazawa, M. 1994 Characean cells as a tool for studying electrophysiological characteristics of plant cells. *Cell Struct. Func.* **19**, 263–278.

Shimmen, T. & Yokota, E. 2004 Cytoplasmic streaming in plants. *Curr. Op. Cell Biol.* **16**, 68–72.

Taiz, L. 1992 The plant vacuole. *J. Exp. Biol.* **172**, 113–122.

Tazawa, M. 1964 Studies on *Nitella* having artificial cell sap. Part I. Replacement of the cell sap with artificial solutions. *Plant Cell Phys.* **5**, 33–43.

Verbelen, J. P. & Tao, W. 1998 Mobile arrays of vacuole ripples are common in plant cells. *Plant Cell Rep.* **17**, 917–920.

Windt, C. W., Vergeldt, F. J., De Jager, P. A. & Van As, H. 2006 MRI of long-distance water transport: a comparison of the phloem and xylem flow characteristics and dynamics in poplar, castor bean, tomato and tobacco. *Plant Cell Environ.* **29**, 1715–1729.